

Discovery of a gas-enshrouded broad-line AGN at $z \sim 7$ QIANQIAO ZHOU,¹ XIN WANG,^{1,2,3} HANG ZHOU,¹ EMANUELE DADDI,⁴ LUIS C. HO,^{5,6} SHENGZHE WANG,^{1,2} RUANCUN LI,⁷ ZUYI CHEN,^{8,9} CHENG CHENG,¹⁰ XIHAN JI,¹¹ YUXUAN PANG,¹ AND MENGTING JU¹¹*School of Astronomy and Space Science, University of Chinese Academy of Sciences (UCAS), Beijing 100049, China*²*National Astronomical Observatories, Chinese Academy of Sciences, Beijing 100101, China*³*Institute for Frontiers in Astronomy and Astrophysics, Beijing Normal University, Beijing 102206, China*⁴*Laboratoire AIM, CEA/DSM-CNRS-Université Paris Diderot, IRFU/Service d’Astrophysique, Bât. 709, CEA Saclay, F-91191 Gif-sur-Yvette Cedex, France*⁵*Kavli Institute for Astronomy and Astrophysics, Peking University, Beijing 100871, China*⁶*Department of Astronomy, School of Physics, Peking University, Beijing 100871, China*⁷*Max-Planck-Institut für extraterrestrische Physik, Gießenbachstraße 1, 85748 Garching bei München, Germany*⁸*Cosmic Dawn Center (DAWN)*⁹*Niels Bohr Institute, University of Copenhagen, Jagtvej 128, 2200 Copenhagen N, Denmark*¹⁰*Chinese Academy of Sciences South America Center for Astronomy, National Astronomical Observatories, CAS, Beijing 100101, China*¹¹*Kavli Institute for Cosmology, University of Cambridge, Madingley Road, Cambridge CB3 0HA, UK*

ABSTRACT

The Lyman-alpha (Ly α) absorption profile in star-forming galaxies serves as a powerful tracer of the extended, dense neutral hydrogen in their surroundings during the Epoch of Reionization (EoR). We report a unique galaxy, A2744-z7DLA, at $z \approx 6.87$ gravitationally lensed by the foreground galaxy cluster Abell 2744, which exhibits both moderate Ly α emission and damped Ly α absorption, suggesting the presence of a dense neutral hydrogen environment. Our analysis suggests that the UV continuum turnover near Ly α is more likely shaped by a damped Ly α system rather than nebular continuum from two photon process. We analyze the physical properties of A2744-z7DLA with spectroscopic and photometric data from the JWST and the HST. The galaxy shows a compact morphology ($r_e \sim 0.3$ kpc) and a broadened H α emission line, suggesting possible AGN activity. The broad component of H α has a FWHM of 2721 ± 200 km s $^{-1}$, corresponding to a black hole mass of $M_{\text{BH}} = 2.90_{-1.28}^{+2.35} \times 10^7 M_{\odot}$ and a black hole-to-stellar mass ratio of $\log(M_{\text{BH}}/M_{\text{stellar}}) = -1.58_{-0.34}^{+0.45}$. The Balmer decrement (H α /H β) yields a dust attenuation of $A_V \approx 1.15 \pm 0.23$, indicating that this system is less dust-rich than some “little red dots”. Furthermore, we perform SED fitting using both stellar and AGN models. The results show that the UV and optical wavelengths are dominated by star-forming regions, while the AGN component contributes primarily at longer wavelengths. This work provides new insights into the interplay between star formation, neutral gas, and potential AGN activity in galaxies during the EoR.

Keywords: Active galactic nuclei (16), Damped Lyman-alpha systems (349), Reionization (1383), High-redshift galaxies (734)

1. INTRODUCTION

The distribution and physical state of the neutral gas surrounding high redshift galaxies provide key insight into their star forming activities and evolutionary processes (Wolfe et al. 2005). A direct tracer of neutral

hydrogen is the 21 cm hyperfine transition; however, the weakness of H I 21cm emission at cosmological distances makes it extremely difficult to detect from individual galaxies (Fernández et al. 2016; Maddox et al. 2021).

An alternative indicator of neutral hydrogen during the Epoch of Reionization (EoR) is the absorption feature of Lyman-alpha (Ly α) emission caused by extended, dense gas surrounding star-forming galaxies (Heintz et al. 2024). Among Ly α absorbers, damped

$\text{Ly}\alpha$ absorption (DLA) systems, with HI column densities $N_{\text{HI}} > 2 \times 10^{20} \text{ cm}^{-2}$, are fundamentally different because the hydrogen in these systems is predominantly neutral (Wolfe et al. 2005). The absorption strength is determined by the density and spatial distribution of neutral hydrogen along the line of sight, making it a useful tool for constraining the characteristics of the high-redshift intergalactic medium (IGM) (Mason et al. 2025). Studying $\text{Ly}\alpha$ absorbers helps to elucidate the relationship between their host galaxies and the surrounding neutral gas (Lofthouse et al. 2023; Mackenzie et al. 2019). Moreover, DLA systems provide valuable insights into the chemical evolution and the interplay between neutral gas and star-forming activity in high-redshift galaxies (Wolfe et al. 2005).

The launch of the James Webb Space Telescope (JWST) has enabled us to explore the DLA during the EoR. So far, JWST/NIRSpec, especially prism spectra, has revealed numerous DLA systems at $z > 5$, which are located in almost fully neutral IGM (Nakane et al. 2024; Tang et al. 2024; Jones et al. 2025a; Kageura et al. 2025; Curti et al. 2025; Witstok et al. 2025). However, due to the low spectral resolution of the prism around $1 \mu\text{m}$, the DLA feature may be degenerate with other features that alter the shape of the UV continuum (Mason et al. 2025). For example, the UV continuum is sampled by only a few pixels, allowing moderate $\text{Ly}\alpha$ emission to contaminate the continuum (Keating et al. 2024; Chen 2024; Jones et al. 2024; Park et al. 2025). Further observations, combined with models that incorporate more realistic distributions of neutral hydrogen gas in ionized bubbles and IGM, are required to robustly constrain the cosmic reionization timeline.

Thanks to the exceptional sensitivity of JWST, a very special kind of galaxy has been discovered—the “little red dots” (LRDs). These are optically red sources with very compact sizes, and their spectra often exhibit broad permitted emission lines ($\text{FWHM} > 1500 \text{ km s}^{-1}$) (Barro et al. 2024; Greene et al. 2024; Labbe et al. 2024; Matthee et al. 2024). Nevertheless, a sample of LRDs with narrow emission lines and without broad $\text{H}\alpha$ lines indicates that the Little Red Dot population may comprise a heterogeneous mixture of sources with different physical natures (Zhang et al. 2025b). Most of the LRDs identified by JWST are located at redshifts $z \sim 4\text{--}8$ or even higher (Tanaka et al. 2025), but the statistical search for LRDs is being extended to $z < 4$ in wide fields (Bisigello et al. 2025; Lin et al. 2025; Ma et al. 2025; Ji et al. 2025a). LRDs exhibit some puzzling properties, such as a significant Balmer break or a V-shaped spectral energy distribution (SED) (e.g., Baggen et al. 2024; Greene et al. 2024; Kokorev et al. 2024; Labbe

et al. 2024; Wang et al. 2025; Setton et al. 2025; Hviding et al. 2025), absorption features superimposed on broad $\text{H}\alpha$ and/or $\text{H}\beta$ emission lines (e.g., Juodžbalis et al. 2024a; Kocevski et al. 2025; Matthee et al. 2024; D’Eugenio et al. 2025; D’Eugenio et al. 2025). Based on multi-epoch observations (Kokubo & Harikane 2025), most LRDs exhibit little variability and X-ray weakness (Ananna et al. 2024; Yue et al. 2024; Lambrides et al. 2024; Maiolino et al. 2025), possibly as a result of super-Eddington accretion onto black holes (Zhang et al. 2025a; Zhou et al. 2025; Ji et al. 2025b).

Thorough analysis of low-redshift analogs of high-redshift LRDs implies an atypical stellar and AGN model (e.g., Ji et al. 2025a; Lin et al. 2025; Lin et al. 2025). Previous studies aimed at explaining the spectroscopic features of LRDs emphasize that the extremely dense gas may cause the V-shaped SED (Inayoshi & Maiolino 2025; Naidu et al. 2025; Ji et al. 2025b; Rusakov et al. 2025; de Graaff et al. 2025; Taylor et al. 2025). Inayoshi & Maiolino (2025) explored how dense gas and AGN activity could account for the Balmer break and absorption features, ensuring that the inferred stellar mass remains consistent with structure formation models (Akins et al. 2025; Inayoshi & Ichikawa 2024). However, Liu et al. (2025) argue that a super-Eddington accretion system can naturally give rise to both the Balmer break and the red optical color, eliminating the need for external gas absorption or dust.

It has occurred to us that the possible physical conditions of LRDs may help explain certain high-redshift DLA systems, as they share some similar features. For instance, GS9422 in the Hubble Ultra Deep Field (HUDF; Beckwith et al. 2006) is a low-mass, compact galaxy. The JWST Advanced Deep Extragalactic Survey (JADES Eisenstein et al. 2023, PIs Rieke and Lützgendorf) has determined its spectroscopic redshift to be 5.943. Several studies have discussed the nature of the UV continuum and $\text{Ly}\alpha$ emission of GS9422 (Terp et al. 2024; Li et al. 2024b; Tacchella et al. 2025; McClymont et al. 2025; Cameron et al. 2024; Katz et al. 2025; Trussler et al. 2025). Li et al. (2024b); Tacchella et al. (2025) agree that an AGN is required to reproduce the UV continuum of GS9422, although Cameron et al. (2024); Katz et al. (2025); Trussler et al. (2025) suggests that nebular emission powered by stellar populations with a top-heavy IMF is also a plausible source. In this work, we present a similar galaxy, A2744-z7DLA, which exhibits both a curved Lyman break and moderate $\text{Ly}\alpha$ emission. In addition, A2744-z7DLA shows broad $\text{H}\alpha$ emission and strong rest-optical lines, along with a compact morphology and blue rest-optical col-

ors. These characteristics make it a compelling system to link with both DLA galaxies and LRDs.

This paper is organized as follows. In Section 2, we provide a brief overview of the observation and data reduction process. Section 3 presents the basic results and analysis of A2744-z7DLA, including its physical properties derived from SED fitting, UV continuum and Ly α features, as well as emission diagnostics. In Section 4, we discuss the results in detail. Finally, the conclusions and future prospects are summarized in Section 5. Throughout this paper, we adopt a Λ CDM cosmology with $\Omega_m = 0.3$, $\Omega_\Lambda = 0.7$, and $H_0 = 70 \text{ km s}^{-1} \text{ Mpc}^{-1}$. The cosmic distances used in this study are calculated using the Cosmology Calculator (Wright 2006).

2. OBSERVATIONS AND DATA REDUCTION

A2744-z7DLA, at a redshift of $z \approx 6.87$, is observed in the lensing field of Abell 2744, showing a Ly α absorption feature along with weak Ly α emission. Abell 2744 is a galaxy cluster at $z = 0.308$ that has been extensively studied through multiwavelength observations. The abundance of archival data, particularly the recent JWST imaging and spectroscopic observations, combined with the magnification effect of the galaxy cluster, enhances our ability to investigate the properties of A2744-z7DLA.

Inspired by the previously discussed GS9422, we aim to identify analogous galaxies in Abell 2744 that exhibit both Ly α emission and a DLA feature. We selected A2744-z7DLA as a candidate using the DAWN JWST Archive (DJA), a repository of public JWST galaxy data reduced with `grizli` (Brammer et al. 2022) and `msaexp` (Brammer 2023).

2.1. JWST/NIRCam and HST photometry

The mosaics for the Abell 2744 NIRCam imaging were processed by the UNCOVER project DR2¹ (Bezanson et al. 2024). A detailed description of the image reduction process is provided in Bezanson et al. (2024). We included data from 7 filters in this research: F115W, F150W, F200W, F277W, F356W, F410M, and F444W. The data were produced using the JWST pipeline version 1.8.4, with the calibration file JWST 0995.PMAP. We displayed the images from JWST/NIRCam in the first column of Figure 2.

To investigate this further, we compute the color indices F277W–F444W, F277W–F356W, and F150W–F200W in AB magnitudes using the photometric catalog from Treu & Paris (2023), and compare them with the LRD candidates (Labbe et al. 2024) in Figure 7.

Table 1. Physical Properties of Galaxy A2744-z7DLA

| Parameters | Values |
|---|--------------------------|
| R.A. [deg] | 3.580446 |
| Decl. [deg] | -30.404990 |
| z_{spec} | 6.87 |
| μ (magnification) | $2.26^{+0.14}_{-0.14}$ |
| r_e [kpc] | 0.36 ± 0.01 |
| Direct spectral results | |
| Av [mag] | 1.15 ± 0.23 |
| β (UV slope) | $-2.46^{+0.03}_{-0.03}$ |
| SFR (H β) [M_\odot/yr] | 13.21 ± 3.94 |
| SED fitting results | |
| $\log(M_*/M_\odot)$ | $8.77^{+0.24}_{-0.11}$ |
| SFR (SED fitting) [M_\odot/yr] | 2.81 ± 0.36 |
| $\log(Z_*/Z_\odot)$ | -1.01 ± 0.02 |
| t_{age} [Myr] | $12.37^{+4.21}_{-1.74}$ |
| Observed emission line ratios | |
| H α /H β | 3.90 ± 0.25 |
| [O III] $\lambda 5007$ /[O III] $\lambda 4363$ | 26.56 ± 9.60 |
| [O III] $\lambda 5007$ /[O II] $\lambda\lambda 3727, 3729$ | > 13.22 |
| [O III] $\lambda 5007$ /H β | 3.11 ± 0.24 |
| [O III] $\lambda 4363$ /H γ | 0.19 ± 0.07 |
| [Ne III] $\lambda 3869$ /[O II] $\lambda\lambda 3727, 3729$ | > 1.79 |
| DLA analyses | |
| $\log \text{EW}_{\text{Ly}\alpha}$ [\mathring{A}] | $1.89^{+0.08}_{-0.07}$ |
| $\log N_{\text{HI}}$ [cm $^{-2}$] | $22.20^{+0.32}_{-0.37}$ |
| Δv [10 3 km s $^{-1}$] | $-14.95^{+3.19}_{-3.11}$ |
| f_c | $0.24^{+0.08}_{-0.05}$ |
| R_{ion} [Mpc] | $1.17^{+0.56}_{-0.47}$ |

NOTE — The effective radius is measured using `GalfitS`, with magnification correction applied. The magnification factor μ is derived from the CATS 4.1 lensing model (Limousin et al. 2016). The star formation rate from H β emission, SFR(H β), is calculated using the relation $\text{SFR}(H\beta) = 4.65 \times 10^{-42} L_{H\beta} [\text{erg s}^{-1}] \times 2.86 [M_\odot \text{ yr}^{-1}]$ (Kennicutt Jr 1998; Chabrier 2003). The stellar mass, $\log(M_*/M_\odot)$, SFR (SED fitting), $\log(Z_*/Z_\odot)$, and t_{age} [Myr] are derived from `Bagpipes` SED fitting. The observed line ratios are reported prior to dust correction. The parameter β denotes the UV continuum slope. All quoted uncertainties correspond to 1σ confidence intervals.

The color of A2744-z7DLA is not as red as that of the LRDs and it does not display a V-shaped SED. A more detailed discussion is provided in Section 4.4. The photometric data from Treu & Paris (2023), including the ACS/WFC (F814W) and WFC3/IR (F105W, F125W, F140W, and F160W) bands, together with the seven JWST/NIRCam bands mentioned above, are shown in Figure 1.

¹ <https://jwst-uncover.github.io/DR2.html#Mosaics>

2.2. JWST/PRISM spectrum

We utilize the low-resolution JWST/NIRSpec PRISM spectra from the UNCOVER project (DR4)² (PIs: Labb   & Bezanson; PID: GO-2561; [Bezanson et al. 2024](#)), to study the continuum and emission line characteristics of A2744-z7DLA ([Price et al. 2025](#)). The observations combine NIRCam imaging (reaching depths of 29.5 to 30 AB magnitude in 8 filters) and low-resolution ($R \approx 100$) NIRSpec/PRISM spectroscopy (19-hour exposures), using strong lensing to probe faint galaxies at redshifts $z > 10$ and during the Epoch of Reionization. We use `msaexp` to do reductions, which still use parts of the STScI pipeline but there are some changes included to increase the data quality ([Brammer 2023](#)).

3. ANALYSIS AND RESULTS

3.1. Morphology fitting

We use **GalfitS** ([Li et al. 2025](#)) to analyze the imaging data. **GalfitS** is a recently developed multiband forward-modeling code that performs self-consistent image decomposition together with SED modeling across multiple bands. This approach allows us to separate the AGN and host contributions even in very compact sources, such as LRDs ([Chen et al. 2025b,a](#); [Ho et al. 2024](#)).

An empirical Point Spread Function (PSF) model is constructed using the PSFEx ([Bertin 2011](#)) program. The procedure begins by running SExtractor ([Bertin & Arnouts 1996](#)) on our science mosaic images to generate a source catalog, which serves as the input for PSFEx. PSFEx builds the PSF model by selecting a sample of bright, unsaturated, and isolated point sources from the catalog.

This empirical approach is essential, as opposed to using a theoretical model. Our final science products are drizzled mosaic images with a refined pixel scale of 0.02''/pixel (for short-wavelength band). In contrast, theoretical PSFs from tools like WebbPSF are typically simulated based on the native detector pixel scale (0.031''/pixel). This significant mismatch in sampling makes it inappropriate to directly apply a theoretical model to our SED fitting.

We tested two models in **GalfitS**: a double S  rsic model and a S  rsic+PSF model. The S  rsic+PSF model provided a better fit to the observed imaging data. In this model, the AGN component is represented by a PSF ([Li et al. 2025](#)), while the galaxy component is modeled with a single S  rsic profile. In addition to the S  rsic profile parameters, we treated the dust extinction

(A_V), stellar mass, and the nebular ionization parameter ($\log U$) as free parameters during the fitting process. No priors were applied to the AGN continuum, meaning the emission from the PSF component remains arbitrary.

The fitting results are shown in Figure 2. It is evident that the S  rsic+PSF model successfully reproduces the observed features of A2744-z7DLA across most bands.

According to the results from **GalfitS**, the galaxy component dominates all seven bands. The PSF component contributes significantly to the central region of A2744-z7DLA, especially in the long wavelength bands (F277W, F356W, F410M, and F444W) as shown in the second and third column of Figure 2. We emphasize that the central PSF cannot be entirely attributed to the AGN in the **GalfitS** modeling. A compact central stellar component could also contribute to the PSF in this region.

We noticed that the model does not fit very well in the F115W, F277W, and F356W bands. In F115W, there may be some overestimation of the PSF model, leading to negative residuals at the center. The images in F277W and F356W exhibit complex structure, suggesting that a single S  rsic profile may not fully describe the host galaxy, which requires further investigation.

3.2. SED fitting

With the help of **Bagpipes** ([Carnall et al. 2018, 2019](#)), we perform broadband spectral energy distribution (SED) fitting of our photometric data from [Treu & Paris \(2023\)](#) and spectroscopic data. Our basic assumptions include an exponentially declining star formation history (SFH) and the Calzetti dust extinction law ([Calzetti et al. 2000](#)), with the visual extinction A_V ranging from 0 to 1.5. In this model, the e-folding timescale parameter τ spans from 0.3 to 10 Gyr, and the stellar metallicity (Z/Z_{\odot}) ranges from 0 to 2.5. The integrated fitting results for stellar mass $\log(M_*/M_{\odot}) = 8.77_{-0.11}^{+0.24}$. The star formation rate, metallicity, and stellar age are presented in Table 1. We also measure the UV slope, $\beta = -2.46_{-0.03}^{+0.03}$, by fitting the SED model spectrum over the rest-frame wavelength range of 1500    to 2600   . The result is consistent with that obtained from a simple power-law fit to the observed spectrum.

We note that **Bagpipes** does not include AGN components, while A2744-z7DLA exhibits a broadened H   emission line, a feature commonly associated with AGN activity. To account for this, we further perform SED fitting using **CIGALE** ([Boquien et al. 2019](#)), which incorporates the **SKIRTOR2016** module ([Stalevski et al. 2012, 2016](#)). However, because this AGN module does not include AGN emission lines, the broad component of the

² <https://jwst-uncover.github.io/DR4.html#Spectra>

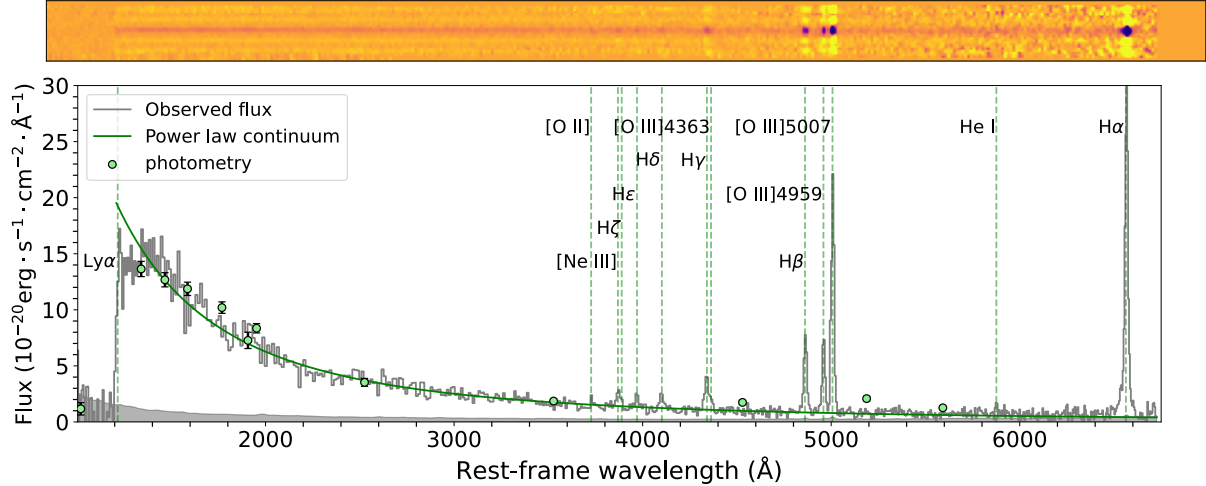


Figure 1. Images and rest frame spectroscopy of A2744-z7DLA. **Top:** The 2D prism spectrum extracted using the `msaexp` pipeline from Gabe Brammer. **Bottom:** The extracted 1D spectrum is shown in gray, with the 1σ error indicated by the light gray shading. Broadband photometry measurements from the literature (Treu & Paris 2023) are included as light green dots with error bars. The light green curve represents the best-fit power law model of the rest-frame UV continuum, spanning $1500 - 2600 \text{ \AA}$. Important emission line wavelengths are marked with vertical dashed lines. It is evident that A2744-z7DLA exhibits a series of prominent Balmer lines and weak Ly α emission.

H α emission is not modeled. The AGN fractions inferred from CIGALE are substantially smaller than the PSF-component fractions derived from GalfitS. In F277W, F356W, and F444W, the AGN fractions are 0.07, 0.06, and 0.10, respectively. Therefore, we infer that the PSF component in the GalfitS decomposition is predominantly contributed by stellar emission.

We also note that CIGALE predicts a very strong Ly α emission line. Given the UV and optical continua, the nebular model appears to favor such a strong Ly α emission, which is not observed in the data.

From CIGALE, the best-fit stellar mass is $\log(M_*/M_\odot) = 8.59 \pm 0.15$, consistent with the result obtained from Bagpipes. The SED models generated by these codes are presented in Figure 3. The figure shows that, at least in the UV and optical bands, the continuum is dominated by star formation rather than AGN emission, which is consistent with the results from GalfitS.

3.3. Emission line fitting

To study the physical properties of the rest-frame optical emission lines, we first fit the continuum near each line with fifth-order polynomial and subtract it from the observed spectrum to isolate the emission features. We then use LMFIT (Newville et al. 2025), to model several individual emission lines with Gaussian profiles. In this analysis, the intrinsic velocity dispersions of H β , H γ , H ϵ , and H δ are constrained to match the value of the narrow H α component. Similarly, the intrinsic velocity dispersions of [O III] $\lambda 4363$ and [O III] $\lambda 4959$ are set to that of [O III] $\lambda 5007$, while the flux ratio between [O III] $\lambda 5007$

and [O III] $\lambda 4959$ is fixed at 2.98. Additionally, the velocity offset of [O III] $\lambda 4363$ and [O III] $\lambda 4959$ is anchored to [O III] $\lambda 5007$. We account for the line-spread function (LSF³) by convolving our model spectrum with Gaussians whose resolution varies with wavelength.

From Figure 4, it is evident that the H α emission line is broadened. We model this line with a two-component Gaussian profile and find that including a broad component significantly improves the fit. To test the robustness of this result, we computed the Bayesian Information Criterion (BIC) for both models: $BIC_{\text{single}} = 176.51$ and $BIC_{\text{two-component}} = 63.74$. The lower BIC value for the two-component model confirms that the broad H α component is real rather than an artifact of overfitting. However, there is not detected broad component in [O III] $\lambda 5007$ and [O III] $\lambda 4959$. We attempted to include a second Gaussian component in the fitting process of [O III] $\lambda 5007$ line. The additional component does not improve the fit, and the BIC value becomes even larger, which indicates that there is no evidence for an outflow-related wing in [O III].

A broad H α emission component is commonly observed in Type I AGN. Although the spectrum of A2744-z7DLA lacks sufficient high-ionization lines to definitively confirm its AGN nature, this remains a plausible scenario. If the observed broad H α emission arises from gas kinematics in the broad-line region (e.g., Greene &

³ We use the fiducial resolving power curves from <https://jwst-docs.stsci.edu/jwst-near-infrared-spectrograph/nirspec-instrumentation/nirspec-dispersers-and-filters>

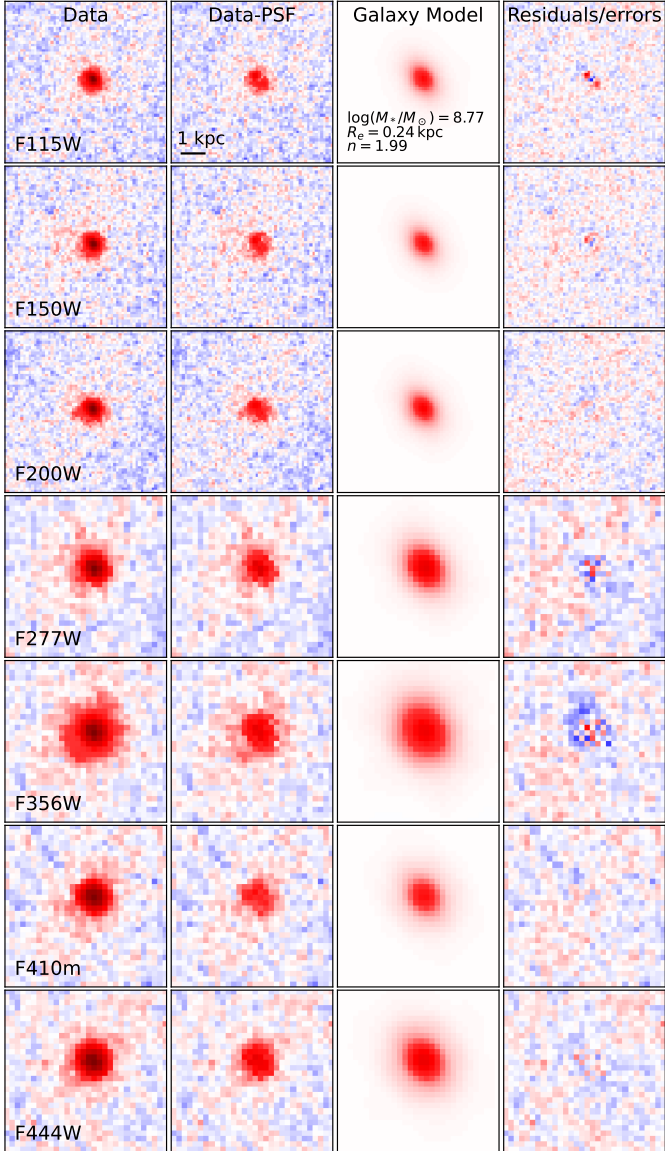


Figure 2. `GalfitS` AGN–host decomposition of A2744-z7DLA. The first column displays the observed images in seven filters; the second column shows data subtracted by PSF model; the third column presents the Sérsic model; and the fourth column shows the residuals divided by the errors. We wrote the stellar mass, effective radius and Sérsic index on the lower left of the panel in first row. The residual images indicate that the model successfully reproduces the observed characteristics of A2744-z7DLA in most bands.

Ho 2005; Kaspi et al. 2005; Larson et al. 2023), and given the well-established correlations between the luminosities of Balmer lines and the continuum luminosity at 5100 Å ($L_{5100} = \lambda L_\lambda$ at $\lambda = 5100$ Å), the black hole mass can be estimated using the broad H α component

following Equation (6) of (Greene & Ho 2005).

$$M_{\text{BH}} = (2_{-0.3}^{+0.4}) \times 10^6 \left(\frac{L_{\text{H}\alpha}}{10^{42} \text{ergs s}^{-1}} \right)^{0.55 \pm 0.02} \times \left(\frac{\text{FWHM}_{\text{H}\alpha}}{10^3 \text{km s}^{-1}} \right)^{2.06 \pm 0.06} M_\odot. \quad (1)$$

However, we caution that the broadening of permitted lines may also arise from electron scattering in dense ionized gas, producing exponential rather than Gaussian line wings (Kokorev et al. 2025), which may lead to an overestimate of the black hole mass. Distinguishing between these mechanisms requires deep, high-resolution spectroscopy, which is beyond the scope of this work.

The luminosity and FWHM of the broad component H α were substituted into the equation above, yielding $M_{\text{BH}} = 2.90_{-1.28}^{+2.35} \times 10^7 M_\odot$ and a black hole–to–stellar mass ratio of $\log(M_{\text{BH}}/M_{\text{stellar}}) = -1.58_{-0.34}^{+0.45}$, which is typical for a supermassive black hole. It should be carefully considered that gas kinematics may not satisfy all the conditions of the standard AGN model, and some studies suggest that the masses might be overestimated (Rusakov et al. 2025; Naidu et al. 2025; Lupi et al. 2024). However, direct dynamical measurement of black hole mass in a lensed LRD at $z = 7.04$ yields a conservative estimate of $M_{\text{BH}}/M_{\text{stellar}} > 2$, suggesting the presence of an almost “naked” black hole (Juodžbalis et al. 2025).

We attempted to place an upper limit on the broad component of H β by tying both the narrow and broad components to those of H α . Although the broad H β component is not as prominent as in H α , the fit is indeed improved. We then applied the formalism from Ho & Kim (2015) using the broad H β component and the monochromatic luminosity at 5100 Å. The resulting black hole masses are $\log M_{\text{BH}} \approx 8.98, 8.51$, and 8.84 for classical bulges, pseudobulges, and the combined sample, respectively—values that are extremely large compared to the stellar mass. Given that the system is more likely stellar-dominated, we do not consider this a meaningful constraint.

We derived a dust extinction of $A_V = 1.15 \pm 0.23$ using the narrow components of both H α and H β . Estimating A_V from the Balmer decrement in AGN systems can be problematic: Kollatschny et al. (2000); Li et al. (2024a) found an anti-correlation between H α /H β and continuum or line flux in a 20-year optical monitoring campaign of the Seyfert 1 galaxy NGC 7603. CLOUDY simulations, theoretical recombination spectra, and SDSS observations consistently suggest that the Balmer decrement is reliable only for BLR regions with high ionization parameter or density at large column densities (Ilić et al. 2012). To minimize these effects, we use only the narrow Balmer components, ensuring that our estimate

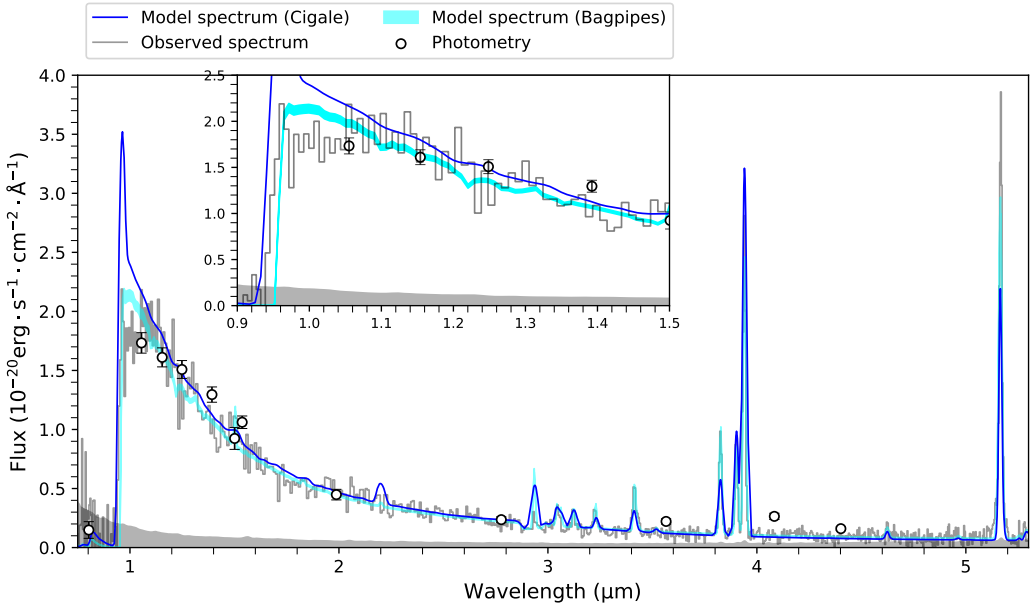


Figure 3. SED fitting results from **CIGALE** and **Bagpipes**. The total model spectra from **CIGALE** and **Bagpipes** are shown as blue and cyan curve. The observed photometric fluxes for the filters F814W, F105W, F125W, F140W, F160W, F115W, F150W, F200W, F277W, F356W, F410M, and F444W are shown as white points. The observed flux and error are represented by the gray curve and shaded region, respectively. We zoom in on the UV turnover part of the spectrum in the upper-right corner of this figure. Both the **CIGALE** and **Bagpipes** models reproduce the UV and optical observations well, but neither fits the curvature at the red end of 1216 Å successfully.

is not driven by BLR emission. However, since we lack evidence for long-term variability in A2744-z7DLA, this result should be interpreted with caution.

We also attempted to place an upper limit on the [N II] $\lambda\lambda 6548, 6584$ lines by subtracting the best-fit H α Gaussian model from the continuum-subtracted spectrum. We then fixed the line width to that of the narrow H α component and fitted the residuals. Due to the limited spectral resolution, we adopted a single Gaussian model for the fit. For the [O II] $\lambda\lambda 3726, 3729$ doublet, we estimate the upper limits of their fluxes by fixing the line width to that of [O III] $\lambda 5007$, as no reliable detection of these lines is present in the observed spectrum. Similarly, we derive the upper limit for He I by fixing the intrinsic line width to that of the narrow H α component and performing a Gaussian fit. Representative fitting results are shown in Figure 4 and summarized in Table 2.

3.4. UV continuum and Ly α emission

A2744-z7DLA exhibits a strong sign of UV turnover, which is commonly observed in DLA systems. However, inspired by the recently widely discussed galaxy GS9422 at $z = 5.943$ (Cameron et al. 2024; Terp et al. 2024; Li et al. 2024b; Tacchella et al. 2025), we considered the nebular continuum as a possible source of the UV continuum in A2744-z7DLA.

For the potential DLA system, we use the same approach as Chen et al. (2024) to construct the model. We modeled the intrinsic continuum with a simple power law fitted over the rest-frame wavelength range of 1500 Å to 2600 Å. We assume that the effect of residual neutral hydrogen within the ionized bubble can be neglected.

The modeling of the DLA system includes the effects of HI column density, velocity offset and covering fraction. The sightline that is covered by the DLA are also taken into account (Chen et al. 2024). The absorbed spectra resemble the Voigt-Hjerting function, and we use the algorithms described in Tasitsiomi (2006) to approximate it.

The remaining photons interact with the neutral Intergalactic Medium (IGM). The foreground neutral hydrogen absorbs photons that have been redshifted to 1216 Å relative to them. We use the same method as Miralda-Escudé (1998) to model the IGM absorption, incorporating necessary corrections based on the Gunn-Peterson effect to calculate the optical depth of Ly α (Heintz et al. 2024).

Since the observed spectrum of A2744-z7DLA shows an inconspicuous Ly α emission line, we add this component to our model. We use a Skew-Normal Function for the Ly α profile to remove the emission on the blue side.

During the fitting process, we convolve the model spectrum with Gaussians of variable resolution to account for the effect of the LSF. The resolution curve

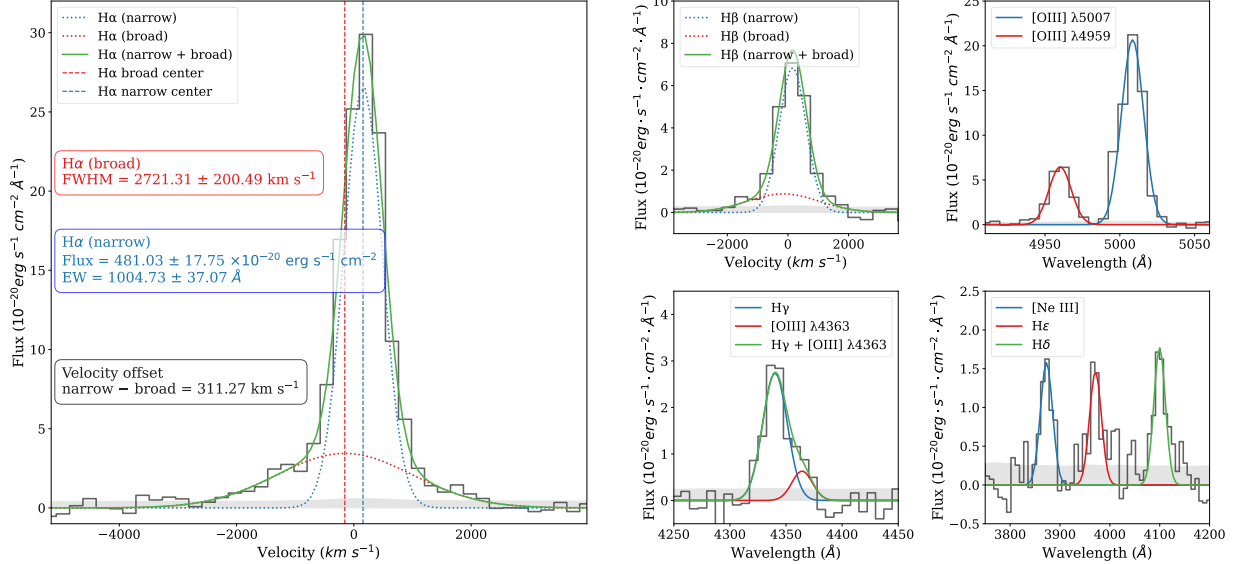


Figure 4. Fitting results of optical emission lines identified in the JWST/NIRSpec spectrum of A2744-z7DLA. The panels show F_λ (in units of $10^{-20} \text{erg} \cdot \text{s}^{-1} \cdot \text{cm}^{-2} \cdot \text{\AA}^{-1}$) as a function of velocity offset or rest-frame wavelength. In the left panel, we showed more detailed information about the two-component Gaussian fitting of H α emission. Relevant measurements, such as line flux and FWHM, are displayed in this panel, using the same color as the corresponding best-fit model. All results presented here are before correction for dust extinction and lensing magnification. Emission-line measurements are summarized in Table 2. A detailed description of the fitting method and a discussion of line ratios are provided in Sections 3.3 and 4.3.

adopted here is the same as that used in Section 3.3. We treated the HI column density of the DLA (N_{HI} , reported in logarithmic form), the velocity offset of the DLA relative to the target galaxy (Δv), the equivalent width of the Ly α emission line ($\text{EW}_{\text{Ly}\alpha}$, reported in logarithmic form), the covering fraction (f_c), and the size of the bubble (R_{ion}) as free parameters. In this model, $\log(N_{\text{HI}}/\text{cm}^{-2})$ ranges from 21 to 24, Δv ranges from -50 to $0 \times 10^4 \text{ km s}^{-1}$, $\log(\text{EW}_{\text{Ly}\alpha}/\text{\AA})$ ranges from -3 to 3 , f_c ranges from 0 to 1 , and R_{ion} ranges from 0.5 to 2 Mpc. The best-fitting values are $\log(\text{EW}_{\text{Ly}\alpha}/\text{\AA}) = 1.89^{+0.08}_{-0.07}$, $\log(N_{\text{HI}}/\text{cm}^{-2}) = 22.20^{+0.32}_{-0.37}$, $\Delta v = -1.50^{+0.32}_{-0.31} \times 10^4 \text{ km s}^{-1}$, $f_c = 0.24^{+0.08}_{-0.05}$, and $R_{\text{ion}} = 1.17^{+0.56}_{-0.47}$ Mpc. The corresponding Ly α flux is measured to be $84.61^{+110.97}_{-41.21} \times 10^{-20} \text{ erg s}^{-1} \text{ cm}^{-2}$. All uncertainties presented here correspond to the 1σ confidence intervals. A full summary of the fitting results obtained from these models is provided in Table 1. The observed absorption profile suggests a very large inflow velocity based on the best-fit velocity offset; however, we caution that this may be affected by the low spectral resolution.

Since the Ly α emission is so weak, we must rule out the possibility that it is a defective pixel. Therefore, we masked the wavelength range from 1210 Å to 1230 Å and repeated the above process. It turns out that the best-fit equivalent width of the Ly α emission line becomes smaller, meanwhile the HI column density of the

DLA and the cover fraction become larger. Thus, the observed Ly α emission is real if we adopt this model.

In order to rule out the possibility that nebular emission, especially the two-photon emission, dominates the UV continuum turnover instead of DLA, we plotted the model spectrum from the CIGALE SED fitting in Figure 5 for comparison. However, without DLA, this model fails to reproduce the UV continuum well. The model spectrum appears much higher than the observed data at the red end of the 1216 Å and exhibits a very strong Ly α emission line.

The fitting results of both the DLA and stellar+nebular emission models are plotted in Figure 5 with green and orange lines, respectively. The green shaded area corresponds to the 1σ uncertainty of the best-fit DLA model. Furthermore, we plot the pure Ly α emission line without the continuum, derived from the DLA model.

4. DISCUSSION

4.1. HI column density and DLA system

DLA systems typically contain high column density HI absorbers, which block the escape of Ly α photons (Wolfe et al. 2005; Vladilo 1999). However, several DLA systems, such as A2744-z7DLA, exhibit weak Ly α emissions. Previous studies during the Cosmic Noon have shown that Lyman-alpha emitters (LAEs) tend to cluster around absorbers with high HI column densities. This seemingly contradictory scenario arises from

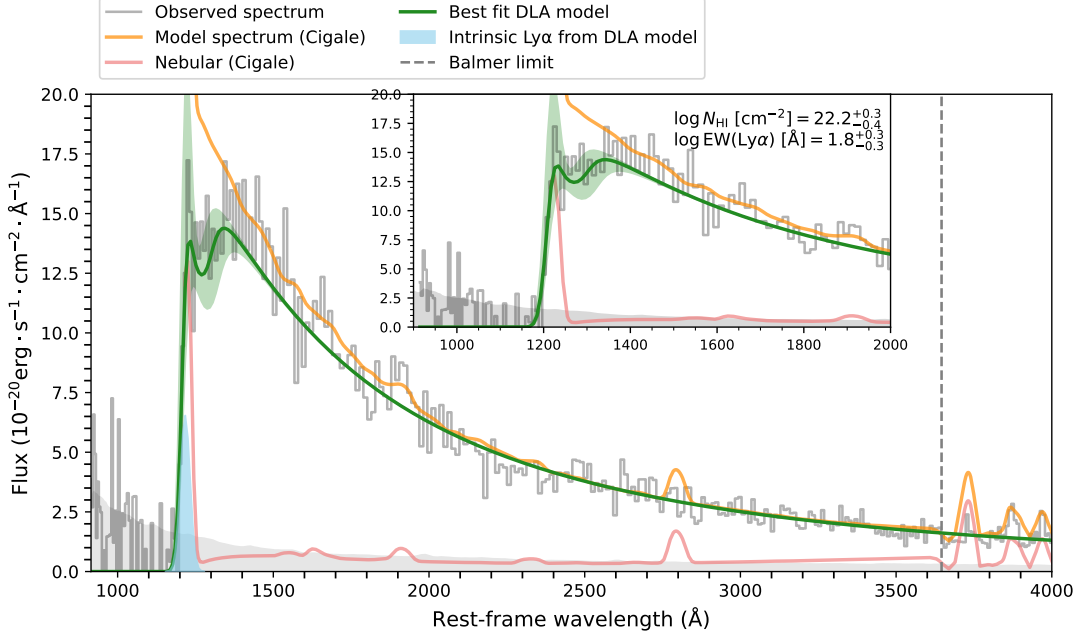


Figure 5. Observed spectroscopic data and best-fit models. The rest-frame NIRSpec/prism 1D spectra and their 1σ uncertainties are shown as gray lines and shaded regions, respectively. The best-fit DLA models and their uncertainties are plotted as green lines and shaded regions. The lower limit of intrinsic Ly α estimated from the DLA model is shaded in sky blue. The model spectrum and nebular components from the CIGALE are plotted in orange and pink, respectively. We also mark the Balmer limit with black vertical lines. We zoomed in on the UV turnover part of the spectrum and wrote the best-fitting HI column density and Ly α flux in the upper-right corner of this figure. Even considering the nebular emission, it is difficult to reproduce both the UV curvature and the steep UV slope β simultaneously, so the DLA absorption is required.

Table 2. Rest-frame optical emission line properties of A2744-z7DLA.

| Emission Line | Observed Flux ^a [$10^{-20} \text{erg} \cdot \text{s}^{-1} \text{cm}^{-2}$] | extinction-corrected flux ^b [$10^{-20} \text{erg} \cdot \text{s}^{-1} \text{cm}^{-2}$] | Rest-frame Equivalent Width [Å] |
|------------------------------------|--|--|------------------------------------|
| H α narrow | 481.03 ± 17.75 | $1175.96^{+279.22}_{-237.80}$ | 1004.73 ± 37.07 |
| H α broad | 218.19 ± 31.54 | $533.80^{+195.44}_{-155.61}$ | 443.57 ± 64.13 |
| [O III] $\lambda 5007$ | 383.73 ± 21.56 | $1232.83^{+407.38}_{-322.90}$ | 425.22 ± 23.89 |
| [O III] $\lambda 4959$ | 128.77 ± 7.24 | $418.47^{+139.55}_{-110.35}$ | 141.71 ± 7.96 |
| H β narrow | 123.48 ± 6.31 | $411.25^{+137.15}_{-108.39}$ | 180.73 ± 0.51 |
| H β broad | 41.91 ± 12.91 | $139.59^{+92.04}_{-64.62}$ | 62.06 ± 0.33 |
| [O III] $\lambda 4363$ | 14.45 ± 5.16 | $55.20^{+42.45}_{-28.44}$ | 12.82 ± 4.58 |
| H γ | 75.33 ± 5.64 | $289.60^{+116.67}_{-87.85}$ | 66.49 ± 4.98 |
| H δ | 51.36 ± 6.04 | $211.12^{+100.93}_{-72.80}$ | 62.18 ± 7.31 |
| H ϵ | 43.72 ± 6.54 | $185.80^{+98.56}_{-69.31}$ | 46.89 ± 7.01 |
| [Ne III] $\lambda 3869$ | 48.42 ± 6.53 | $210.52^{+108.98}_{-76.88}$ | 39.95 ± 5.39 |
| [O II] $\lambda\lambda 3726, 3729$ | < 30.66 | < 136.98 | - |
| [N II] $\lambda\lambda 6548, 6584$ | < 10.02 | < 29.13 | - |
| He I $\lambda 5877$ | < 20.50 | < 55.682 | - |

NOTE — The observed line fluxes and equivalent widths are measured from our emission line analyses of the NIRSpec/MSA prism spectrum with the LMFIT software (see 4 for details).

^a The observed line fluxes and upper limits before the corrections of dust extinction and lensing magnification.

^b The intrinsic line fluxes and upper limits after the corrections of dust extinction. We adopt $A_V = 1.15 \pm 0.23$ measured from the Balmer decrement (H α /H β).

the complex structure of the circumgalactic medium (CGM), which is patchy and inhomogeneous (Lofthouse et al. 2023; Khanlari et al. 2024).

Additionally, Ly α emitters during cosmic noon are relatively small compared to galaxies with similar UV luminosities (Kim et al. 2025). This suggests that a compact morphology plays a crucial role in facilitating the escape of Ly α photons. Since the size-luminosity relation at redshift $z \sim 3 - 4$ is consistent with that of local Green Pea galaxies, the trend of LAEs being more compact does not evolve with redshift. A2744-z7DLA, a Ly α emitter during the reionization epoch, features a compact size and outflows. This object can help us extend our understanding of this relationship to higher redshifts and potentially uncover the underlying mechanisms.

A2744-z7DLA shows both DLA and Ly α emission. We fit the continuum with two models. One incorporates both DLA, Ly α emission and IGM absorption, the other is considered a nebular continuum, Ly α emission and IGM absorption. It appears that the former can reproduce the UV spectrum better. We find that the DLA model does not constrain the ionized bubble size well, indicating that the UV turnover is dominated by nearby neutral H I outside the bubble and is therefore insensitive to R_{ion} . However, A2744-z7DLA exhibits a very faint Balmer jump, resembling a feature of free-bound emission, which typically dominates the nebular continuum. Therefore, we cannot rule out the contribution of nebular emission to the continuum.

However, it is important to note that high resolution data is required to better distinguish the effect of DLA versus IGM when modeling the absorber and estimating the intergalactic neutral hydrogen fraction. As discussed by Huberty et al. (2025), degeneracies between the DLA column density (N_{DLA}) and the neutral fraction of the IGM (x_{HI}) can compromise the accuracy of such measurements. In addition, when only a single absorption component is fitted, low-resolution spectra may result in an overestimation of N_{DLA} (Ellison et al. 2009).

4.2. AGN diagnostics

We plot AGN diagnostic diagrams to assess the likelihood that our object hosts an AGN. In the left panel of Figure 4.2, we show the classical N2-BPT diagram from Kewley et al. (2001) and Kauffmann et al. (2003), along with comparison samples from Maiolino et al. (2024) and Übler et al. (2023), as well as GS9422 from Cameron et al. (2024). We adopt [O III] $\lambda 5007$, H β , H α , and [N II] $\lambda 6583$ measurements from JWST/NIRSpec G395H/F290LP, while [Ne III] $\lambda 3869$ and [O II] $\lambda\lambda 3727, 3729$ are taken from

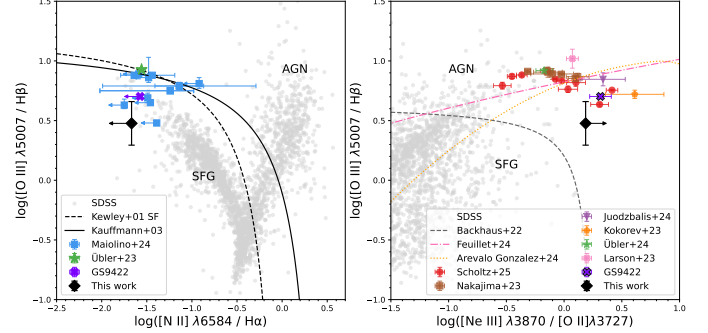


Figure 6. Emission-line diagnostics of star formation/AGN activity. **Left:** N2-BPT diagram from Kewley et al. (2001) and Kauffmann et al. (2003), along with comparison samples from Maiolino et al. (2024) and Übler et al. (2023), marked with purple squares and a green star. Emission lines of GS-9422 from Cameron et al. (2024) are shown with a purple cross. Our object is marked with a black diamond. **Right:** The relation between [O III] $\lambda 5007$ /H β and [Ne III] $\lambda 3869$ /[O II] $\lambda\lambda 3727, 3729$ (OHNO). We compare our object with narrow-line AGNs at high redshift (Scholtz et al. 2025), galaxies at redshifts $z = 4 - 10$ discovered by JWST (Nakajima et al. 2023), high-redshift overmassive black holes and broad-line AGNs (Juodžbalis et al. 2024b; Kokorev et al. 2023a; Übler et al. 2024; Larson et al. 2023), as well as GS9422 (Cameron et al. 2024).

G235M/F170LP. A2744-z7DLA falls within the star-forming galaxy (SFG) region in this panel, although high-redshift AGN samples often lie near the boundary of this classification. The right panel presents the OHNO diagram, with demarcation curves from Backhaus et al. (2022), Feuillet et al. (2024), and Gonzalez et al. (2025). According to the Backhaus et al. (2022) criteria, our galaxy lies within the AGN region. All emission-line measurements used in this section correspond to the narrow components only.

However, some recent works suggest that commonly used AGN diagnostics may not distinguish star forming galaxies and accreting black holes very well. Cleri et al. (2025) suggest that AGN narrow-line regions and star-forming H II regions occupy strongly overlapping regions in all common strong-line diagnostic diagrams, and low-metallicity AGN naturally produce strong-line ratios that are indistinguishable from extreme star-forming populations. Richardson et al. (2025) pointed that many traditional optical diagnostics such as [O III]/H β vs [N II]/H α perform very poorly for dwarf galaxies. Therefore, we cannot rule out the possibility that the narrow lines of A2744-z7DLA originate from the AGN narrow-line region, or that they are dominated by the ISM in the host galaxy.

4.3. Physical conditions

We derive the electron temperature (T_e) from the [O III] $\lambda 4363$ emission line. We adopt the relation $R_{O3} = \frac{I(4959) + I(5007)}{I(4363)}$ and calculate $T_e([O_{III}]) = 0.7840 - 0.0001357R_{O3} + \frac{48.44}{R_{O3}}$, where T_e is expressed in units of 10^4 K (Pérez-Montero 2017).

This empirical relation assumes an electron density of $n_e = 100 \text{ cm}^{-3}$ and is valid for T_e in the range 0.7 to $2.5 \times 10^4 \text{ K}$. A2744-z7DLA exhibits a $[\text{O III}] \lambda 4363$ emission line blended with $\text{H}\gamma$, resulting in a T_e of $2.4 \times 10^4 \text{ K}$. Using Equation (1) from Pérez-Montero et al. (2021), we estimate the metallicity of A2744-z7DLA to be $12 + \log(\text{O/H}) \approx 7.48$. Although these electron temperature and metallicity values may not be accurate for the low SNR of $[\text{O III}] \lambda 4363$, this estimate still indicates the extremely high electron temperature and metal-poor narrow line region (NLR).

Several studies of LRDs have reported exceptionally high $I(\lambda 4363)/I(\lambda 5007)$ ratios (Kokorev et al. 2023b; Jones et al. 2025b). According to Jones et al. (2025b), such elevated $[O\ III]\ \lambda 4363/[O\ III]\ \lambda 5007$ values may arise from a multiphase ISM—containing both diffuse and dense gas—or from extremely high electron temperatures ($T_e > 10^5$ K). Furthermore, the unusually large $[O\ III]\ \lambda 4363/H\gamma$ ratio suggests that the AGN not only ionizes and overheats the gas, but that the host galaxy must also contain gas with very high densities. For the source discussed by Jones et al. (2025b), the required gas density is on the order of $10^7\ cm^{-3}$.

4.4. Comparison with red compact sources

4.4.1. *Color Selection*

Inspired by the peculiarities of A2744-z7DLA, we compare it with other galaxies from the UNCOVER program (Weaver et al. 2024), focusing on their color and morphology, particularly the LRDs candidates. We adopt the criteria outlined in Labbe et al. (2024); Labb   et al. (2023) and Greene et al. (2024). The goal of this selection is to identify objects that exhibit a red continuum slope in the rest-frame optical while also showing significant emission in the rest-UV, referred to as the “V-shape” color selection.

We first apply a cut of $\text{SNR}_{\text{F444W}} > 14$ and $m_{\text{F444W}} < 27.7$ mag to select well-detected sources. An object is considered to have red color and compact size if it satisfies all of the following criteria:

$$red1 = (\text{F115W} - \text{F150W} < 0.8)$$

$$red2 = (\text{F150W} - \text{F200W} < 0.8)$$

$$compact = f_{F444W}(0.4'')/f_{F444W}(0.2'') < 1.7$$

In Figure 7, we present the well-detected red galaxies from the UNCOVER program. The 17 targets that sat-

isfy the $(red1|red2)$ and *compact* criteria are highlighted with star symbols, while A2744-z7DLA is marked with a diamond. We also plot GS9422 with photometric data from [Tacchella et al. \(2025\)](#) for comparison.

Moreover, as noted by Greene et al. (2024); Hainline et al. (2024), brown dwarf stars are a major source of contamination in such selections. To mitigate this issue, Greene et al. (2024) introduced updated NIRCam-only selection criteria. These criteria incorporate the F277W–F356W color to identify SEDs with genuinely red continuum slopes, rather than objects whose colors are dominated by spectral breaks or emission lines. Overall, an object is considered red and compact only if it simultaneously meets all of the following four criteria:

compact red :

$$(-0.5 < F115W - F200W < 1.0)$$

(F277W – F444W > 1.0)

(F277W – F356W > 0.7)

$$compact = f_{F444W}(0.4'')/f_{F444W}(0.2'') < 1.5$$

We show these criteria in Figure 7 using dashed lines. While A2744-z7DLA satisfies the compactness requirement, it does not meet the “V-shape” color selection. Nevertheless, A2744-z7DLA clearly lies between the robust LRD candidates and the bulk of the catalog galaxies, occupying a similar region in the color–color space as GS9422, which may suggest comparable physical conditions.

4.4.2. Host galaxy

Recent observations reveal that many LRDs exhibit diffuse emission surrounding their compact, point-like centers (Chen et al. 2025b; Rinaldi et al. 2025). Further studies suggest that this diffuse component may trace both the accretion of halo gas and its subsequent conversion into stars (Chen et al. 2025a).

Using `GalfitS` to decompose the AGN and host galaxy of our source, we compare it with previous studies of high-redshift AGN host galaxies. According to Li et al. (2025), luminous blue quasars ($L_{5100} \gtrsim 10^{45} \text{ erg s}^{-1}$) reside in bulge-dominated galaxies (Sérsic index $n \approx 5$), while fainter red quasars inhabit disk-like galaxies (with $n \approx 1$). Based on the SED results, A2744-z7DLA is classified as a fainter source, with a Sérsic index of $n = 1.99$, which is closer to the red quasars. Additionally, red quasars tend to have a higher black hole-to-stellar mass ratio, suggesting the growth of black holes is faster than the growth of their host galaxies. Our source shows $\log(M_{\text{BH}}/M_{\text{stellar}}) = -1.58_{-0.34}^{+0.45}$, also

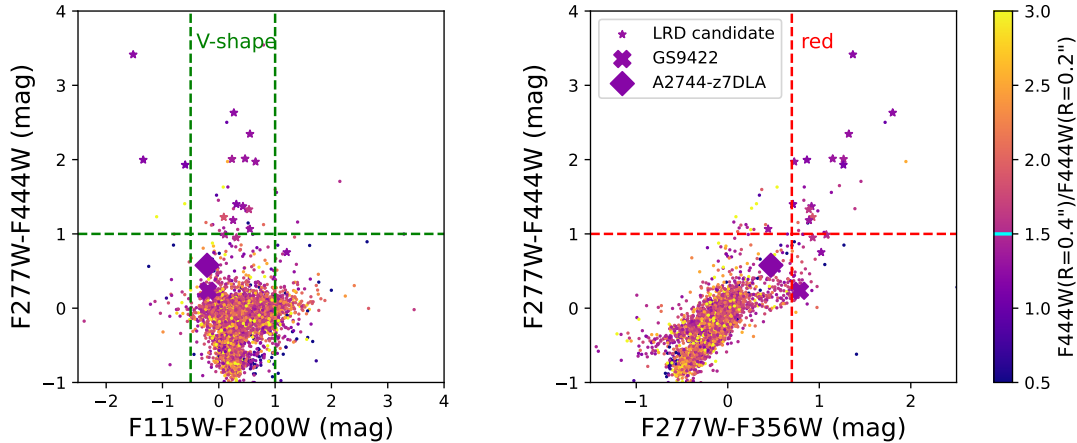


Figure 7. High-redshift red galaxies from the UNCOVER program. The smallest points represent sources from the UNCOVER catalog (Weaver et al. 2024), selected with $F444W < 27.7$ mag and $S/N > 14$ in the $F444W$ band. Star symbols denote Little Red Dot (LRD) candidates from Greene et al. (2024), cross symbol represent GS9422 from Tacchella et al. (2025) while the diamond indicates the position of A2744-z7DLA, the galaxy presented in this work. **Left:** NIRCam color-color diagram of $F277W - F444W$ versus $F115W - F200W$, used to identify galaxies with blue rest-frame UV continua and red rest-frame optical continua—characteristic of a “V-shaped” spectral energy distribution (SED). The vertical dashed lines mark $F115W - F200W = -0.5$ and $F115W - F200W = 1.0$, and the horizontal line indicates $F277W - F444W = 1.0$. **Right:** NIRCam color-color diagram of $F277W - F444W$ versus $F277W - F356W$, designed to select galaxies with red optical continua by applying color cuts between adjacent filters. The vertical line marks $F277W - F356W = -0.7$, and the horizontal line again indicates $F277W - F444W = 1.0$. In both panels, all points are color-coded by the flux ratio $F444W(R = 0.4'')/F444W(R = 0.2'')$, which is used to identify compact sources. The horizontal line in the color bar denotes a flux ratio of 1.5. All selection criteria follow those defined in Greene et al. (2024). Notably, A2744-z7DLA appears to lie between the reliable LRD candidates and the bulk of the catalog galaxies.

between these two values, indicating a potential transitional stage. Lastly, while lower luminosity red quasars show a broad range of UV slopes ($\beta \approx -2$ to 4), luminous blue quasars have a narrow range ($\beta \approx 1.4$). A2744-z7DLA’s steep UV slope aligns with the characteristics of fainter quasars.

Chen et al. (2025b) examines the properties of eight high-redshift LRDs, finding a host galaxy in only one, while four show extended, off-centered emission, possibly from starlight. Chen et al. (2025a) also observed significant extended emission in many LRDs, some of which can be explained by stellar models, while others suggest nebular emission. A2744-z7DLA exhibits a more dominant stellar component and likely nebular emission. We propose that A2744-z7DLA may represent a more evolved stage compared to typical LRDs, in which the AGN contribution is less dominant while the host galaxy plays a larger role, although the underlying process of stellar mass assembly remains consistent.

4.4.3. Black hole mass

We further considered additional physical properties commonly used to characterize AGNs. In the left panel of Figure 8, we present the estimated black hole mass, $\log(M_{\text{BH}}/M_{\odot})$, and bolometric luminosity, $\log L_{\text{bol}}$, for our object, and compare them with other high-redshift galaxies and recently discovered LRDs. The black hole

mass is derived from Equation 3.3, while the bolometric luminosity and the stellar mass are obtained from Bagpipes SED fitting. Dashed lines indicate Eddington ratios of 1, 0.1, and 0.01. The Eddington ratio exhibited by A2744-z7DLA falls between 0.01 and 0.1, consistent with most previous studies.

In the right panel of Figure 8, we show $\log(M_{\text{BH}}/M_{\odot})$ versus $\log(M_{*}/M_{\odot})$ for our object. A2744-z7DLA lies close to the black hole mass–stellar mass relation for $z = 4$ –7 AGNs from Li et al. (2025) (green dashed line):

$$\log\left(\frac{M_{\text{BH}}}{M_{\odot}}\right) = 1.29 + 0.70 \log\left(\frac{M_{*}}{M_{\odot}}\right) \quad (2)$$

The local black hole mass–stellar mass relation, as estimated by Zhuang & Ho (2023), is also shown. It has been known that newly discovered high-redshift AGN tend to be overmassive relative to the stellar mass of their host galaxies, which cannot be explained entirely by the selection effect (e.g., Harikane et al. 2023; Übler et al. 2023; Furtak et al. 2024; Ji et al. 2025b; Juodžbalis et al. 2024b). Recent JWST observations suggest that such black holes are overmassive by a factor of ~ 10 –100 compared to local galaxies of similar stellar mass, and the inferred high- z BH-to-stellar mass relation is significantly different from that in the local universe (Pacucci et al. 2023). For A2744-z7DLA at $z = 6.87$, the results

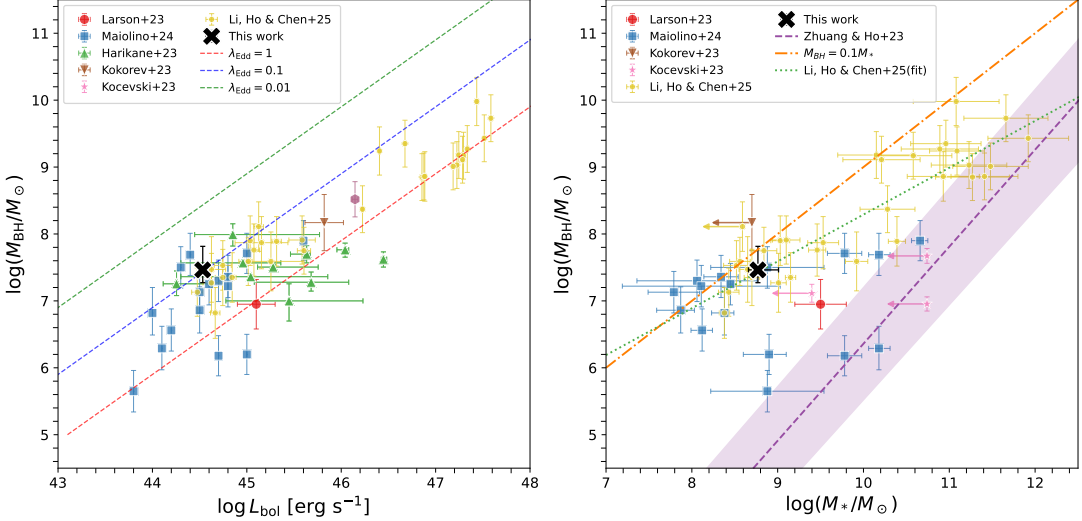


Figure 8. **Left:** Relation between bolometric luminosity and black hole mass. We compare A2744-z7DLA with previously reported high-redshift AGNs and LRDs, including accreting supermassive black holes from Larson et al. (2023); Maiolino et al. (2024), faint high-redshift AGNs from Harikane et al. (2023); Kocevski et al. (2023), a massive black hole in a low-metallicity AGN from Übler et al. (2023), a lensed galaxy with its quiescent companion from Kokorev et al. (2023a), and a comprehensive AGN sample from several JWST surveys from Li et al. (2025). Our measurement is shown as a black cross. The orange, blue, and green dashed lines indicate Eddington ratios of 1, 0.1, and 0.01, respectively. Note that the bolometric luminosity of A2744-z7DLA is estimated from `Bagpipes` SED fitting; therefore, its uncertainty is not displayed. **Right:** Black hole-to-stellar mass relation. The markers correspond to the same samples as in the left panel. The purple dashed line represents the best-fit relation that evolves to $z = 0$ from Zhuang & Ho (2023), while the green dashed line corresponds to the linear fit result from Li et al. (2025). The orange dashed line marks the relation $M_{\text{BH}} = 0.1 M_{*}$. Note that we use the result from `Bagpipes` as the stellar mass of A2744-z7DLA. The results indicate that A2744-z7DLA hosts a rapidly growing massive black hole, consistent with other comparison samples.

indicate the presence of a rapidly growing massive black hole, similar to other comparison samples.

4.5. Massive accreting black hole

According to the `GalFitS` results, A2744-z7DLA contains an AGN component, with an inferred black hole mass of $\sim 2.9 \times 10^7, M_{\odot}$. Given the presence of a DLA system dominating the nearest absorption, dense gas is likely located in the vicinity of, or within, the galaxy.

Widely accepted models of the “Little Red Dots” suggest that cool gas contributes to the formation of the “V-shaped” SED. Lin et al. (2025) proposed that gas with temperatures of $T \sim 5000\text{--}6000\text{K}$ enveloping the central SMBH produces thermalized emission. Inayoshi & Maiolino (2025) hold that a Balmer break can arise in AGN spectra if the accretion disk is deeply shrouded in dense neutral gas clumps. In these regions, collisions excite hydrogen atoms to the $n=2$ state, enabling efficient absorption of the AGN’s continuum emission at wavelengths just below the Balmer limit. The UV band is likely dominated by either an AGN continuum or a young stellar population, and is sometimes absorbed by DLA systems (Ji et al. 2025b). A2744-z7DLA does not exhibit a Balmer break in the optical band, indicating an absence of thermalized emission from the warm neu-

tral medium. However, the presence of cool gas induces curvature in the UV continuum.

Silk et al. (2024) proposed a hypothesis on how feedback influences star formation in star-forming galaxies hosting an AGN. Whether the feedback is positive or negative (i.e., whether cooling is effective or ineffective) depends on the column density of cooled gas behind shocks, because the column density within a galaxy regulates the relative timescales of dynamical processes and cooling, thereby influencing the effectiveness of SMBH feedback on their host galaxies. This model implies that the black hole grows and the AGN activity rises first, subsequently triggering star formation and ultimately suppressing it. A2744-z7DLA exhibits dominant stellar emission, along with a broad H α component indicating the presence of an AGN. It also shows a moderate star formation rate, consistent with the transitional phase predicted by this model.

In summary, the most plausible interpretation for our source is that the broad component of the H α emission line is produced by a supermassive black hole (SMBH) accreting dense gas in its immediate surroundings, while the host galaxy has experienced significant star-forming activity. This scenario is consistent with the models

proposed by Inayoshi & Maiolino (2025) and Silk et al. (2024).

5. CONCLUSION

We report the discovery of a peculiar galaxy in the epoch of cosmic reionization, A2744-z7DLA, located in the A2744 field. We analyzed the morphology of this object using both **GALFIT** and **GalfitS**, finding that it exhibits a very compact structure. The morphological decomposition analysis indicates that A2744-z7DLA contains a central PSF component. When compared with the SED fitting results from **Bagpipes** and **CIGALE**, this component is likely dominated by stellar emission, particularly in the rest-frame UV bands, whereas any AGN contribution becomes more significant only at longer wavelengths.

Its UV continuum shows Damped Lyman-alpha (DLA) absorption features, along with moderate Ly α emission, suggesting the presence of high-density neutral hydrogen (HI) along the line of sight.

A2744-z7DLA exhibits a relatively red color and compact morphology, but lacks the typical “V-shaped” spectral profile, and thus would not be classified as the “Little Red Dot” (LRD) candidate. In color space, it is situated between the majority of reionization-era galaxies and LRDs. The galaxy also exhibits a very high electron temperature and low metallicity, indicating an early evolutionary stage with limited dust enrichment, although it may represent a more evolved phase compared to typical LRDs.

The H α emission line of A2744-z7DLA exhibits a broad component, and the galaxy falls within the AGN region on the OHNO diagnostic diagram, suggesting it may be a Type I AGN. We estimate the FWHM of the broad component to be approximately 2721 km s $^{-1}$, corresponding to a black hole mass of $M_{\text{BH}} = 2.90^{+2.35}_{-1.28} \times 10^7 M_{\odot}$. We show the relations between bolometric luminosity and black hole mass, as well as the black hole-to-stellar mass relation, finding that A2744-z7DLA is consistent with other high-redshift AGNs and LRDs. These results support the scenario in which A2744-z7DLA is in an active black hole mass assembly phase. Its central supermassive black hole is likely accreting

high-density neutral gas, which gives rise to the observed broadening of the emission lines.

Future observations will be essential to assess the AGN interpretation for this source. High-resolution spectroscopy would enable a more definitive search for broad-line components or high-ionization emission features such as C IV or He II. Such observations would provide critical evidence to either support or rule out the presence of an AGN in this compact system.

¹ We thank the anonymous referee for very constructive
² comments that help improve the quality of this paper.
³ This work is supported by the National Key R&D Pro-
⁴ gram of China No.2025YFF0510603, the National Nat-
⁵ ural Science Foundation of China (grant 12373009), the
⁶ CAS Project for Young Scientists in Basic Research
⁷ Grant No. YSBR-062, the China Manned Space Pro-
⁸ gram with grant no. CMS-CSST-2025-A06, and the
⁹ Fundamental Research Funds for the Central Univer-
¹⁰ sities. XW acknowledges the support by the Xiaomi
¹¹ Young Talents Program, and the work carried out,
¹² in part, at the Swinburne University of Technology,
¹³ sponsored by the ACAMAR visiting fellowship. LCH
¹⁴ was supported by the National Science Foundation of
¹⁵ China (12233001) and the China Manned Space Pro-
¹⁶ gram (CMS-CSST-2025-A09). The authors sincerely
¹⁷ thank the UNCOVER team (PIs: Labb   & Bezanson;
¹⁸ PID: GO-2561) for developing their observing program
¹⁹ with a non-proprietary period.

DATA AVAILABILITY

Some of the data presented in this article were obtained from the Mikulski Archive for Space Telescopes (MAST) at the Space Telescope Science Institute. The specific observations analyzed in this study can be accessed via doi: 10.17909/9chn-9q11. The data collection DOI was generated using the MAST DOI service⁴.

Software: **GalfitS** (Li et al. 2025), **Bagpipes** (Carnall et al. 2018, 2019), **LMFIT** (Newville et al. 2025), **CIGALE** (Boquien et al. 2019), **msaexp** (Brammer 2023), **grizli** (Brammer et al. 2022), **PSFEx** (Bertin 2011), **SExtractor** (Bertin & Arnouts 1996)

REFERENCES

Akins, H. B., Casey, C. M., Lambrides, E., et al. 2025,

ApJ, 991, 37, doi: 10.3847/1538-4357/ade984

⁴ <https://archive.stsci.edu/publishing/doi>

Ananna, T. T., Bogd  ,   , Kov  cs, O. E., Natarajan, P., & Hickox, R. C. 2024, The Astrophysical Journal Letters, 969, L18

Backhaus, B. E., Trump, J. R., Cleri, N. J., et al. 2022, The Astrophysical Journal, 926, 161

Baggen, J. F., van Dokkum, P., Brammer, G., et al. 2024, *The Astrophysical Journal Letters*, 977, L13

Barro, G., Pérez-González, P. G., Kocevski, D. D., et al. 2024, *The Astrophysical Journal*, 963, 128

Beckwith, S. V., Stiavelli, M., Koekemoer, A. M., et al. 2006, *The Astronomical Journal*, 132, 1729

Bertin, E. 2011, in *Astronomical data analysis software and systems xx*, Vol. 442, 435

Bertin, E., & Arnouts, S. 1996, *Astronomy and astrophysics supplement series*, 117, 393

Bezanson, R., Labbe, I., Whitaker, K. E., et al. 2024, *ApJ*, 974, 92, doi: [10.3847/1538-4357/ad66cf](https://doi.org/10.3847/1538-4357/ad66cf)

Bezanson, R., Labbe, I., Whitaker, K. E., et al. 2024, *The Astrophysical Journal*, 974, 92, doi: [10.3847/1538-4357/ad66cf](https://doi.org/10.3847/1538-4357/ad66cf)

Bisigello, L., Rodighiero, G., Fotopoulou, S., et al. 2025, arXiv preprint arXiv:2503.15323

Boquien, M., Burgarella, D., Roehlly, Y., et al. 2019, *Astronomy & Astrophysics*, 622, A103

Brammer, G. 2023, *msaexp: NIRSpec analysis tools*, 0.6.17, Zenodo, doi: [10.5281/zenodo.7299500](https://doi.org/10.5281/zenodo.7299500)

Brammer, G., Strait, V., Matharu, J., & Momcheva, I. 2022, *grizli*, 1.5.0, Zenodo, doi: [10.5281/zenodo.6672538](https://doi.org/10.5281/zenodo.6672538)

Calzetti, D., Armus, L., Bohlin, R. C., et al. 2000, *The Astrophysical Journal*, 533, 682

Cameron, A. J., Katz, H., Witten, C., et al. 2024, *Monthly Notices of the Royal Astronomical Society*, stae1547

Carnall, A. C., McLure, R. J., Dunlop, J. S., & Davé, R. 2018, *Monthly Notices of the Royal Astronomical Society*, 480, 4379–4401, doi: [10.1093/mnras/sty2169](https://doi.org/10.1093/mnras/sty2169)

Carnall, A. C., McLure, R. J., Dunlop, J. S., et al. 2019, *Monthly Notices of the Royal Astronomical Society*, 490, 417–439, doi: [10.1093/mnras/stz2544](https://doi.org/10.1093/mnras/stz2544)

Chabrier, G. 2003, *Publications of the Astronomical Society of the Pacific*, 115, 763

Chen, C.-H., Ho, L. C., Li, R., & Inayoshi, K. 2025a, *The Physical Nature of the Off-centered Extended Emission Associated with the Little Red Dots*. <https://arxiv.org/abs/2505.03183>

Chen, C.-H., Ho, L. C., Li, R., & Zhuang, M.-Y. 2025b, *The Astrophysical Journal*, 983, 60

Chen, H. 2024, *Monthly Notices of the Royal Astronomical Society: Letters*, 528, L33

Chen, Z., Stark, D. P., Mason, C., et al. 2024, *Monthly Notices of the Royal Astronomical Society*, 528, 7052

Cleri, N. J., Olivier, G. M., Backhaus, B. E., et al. 2025, *ApJ*, 994, 146, doi: [10.3847/1538-4357/ae0f17](https://doi.org/10.3847/1538-4357/ae0f17)

Curti, M., Witstok, J., Jakobsen, P., et al. 2025, *Astronomy & Astrophysics*, 697, A89

de Graaff, A., Rix, H.-W., Naidu, R. P., et al. 2025, *A&A*, 701, A168, doi: [10.1051/0004-6361/202554681](https://doi.org/10.1051/0004-6361/202554681)

D'Eugenio, F., Maiolino, R., Perna, M., et al. 2025, arXiv preprint arXiv:2503.11752

D'Eugenio, F., Juodžbalis, I., Ji, X., et al. 2025, *MNRAS*, doi: [10.1093/mnras/staf2117](https://doi.org/10.1093/mnras/staf2117)

Eisenstein, D. J., Willott, C., Alberts, S., et al. 2023, arXiv preprint arXiv:2306.02465

Ellison, S. L., Murphy, M. T., & Dessauges-Zavadsky, M. 2009, *Monthly Notices of the Royal Astronomical Society*, 392, 998

Fernández, X., Gim, H. B., Van Gorkom, J., et al. 2016, *The Astrophysical Journal Letters*, 824, L1

Feuillet, L. M., Meléndez, M., Kraemer, S., et al. 2024, *The Astrophysical Journal*, 962, 104

Furtak, L. J., Labbé, I., Zitrin, A., et al. 2024, *Nature*, 628, 57

Gonzalez, F. A., Braun, T., Trussler, J., et al. 2025, *Monthly Notices of the Royal Astronomical Society*, staf1836

Greene, J. E., & Ho, L. C. 2005, *The Astrophysical Journal*, 630, 122

Greene, J. E., Labbe, I., Goulding, A. D., et al. 2024, *The Astrophysical Journal*, 964, 39

Hainline, K. N., Helton, J. M., Johnson, B. D., et al. 2024, *The Astrophysical Journal*, 964, 66

Harikane, Y., Zhang, Y., Nakajima, K., et al. 2023, *The Astrophysical Journal*, 959, 39

Heintz, K. E., Watson, D., Brammer, G., et al. 2024, *Science*, 384, 890

Ho, L., Li, R., Chen, C., & Zhuang, M. 2024, 45th COSPAR Scientific Assembly. Held 13-21 July, 45, 1419

Ho, L. C., & Kim, M. 2015, *ApJ*, 809, 123, doi: [10.1088/0004-637X/809/2/123](https://doi.org/10.1088/0004-637X/809/2/123)

Huberty, M., Scarlata, C., Hayes, M. J., & Gazagnes, S. 2025, arXiv preprint arXiv:2501.13899

Hviding, R. E., de Graaff, A., Miller, T. B., et al. 2025, *A&A*, 702, A57, doi: [10.1051/0004-6361/202555816](https://doi.org/10.1051/0004-6361/202555816)

Ilić, D., Popović, L., La Mura, G., Ciroi, S., & RLi, Sha-Shaafanelli, P. 2012, *Astronomy & Astrophysics*, 543, A142

Inayoshi, K., & Ichikawa, K. 2024, *The Astrophysical Journal Letters*, 973, L49

Inayoshi, K., & Maiolino, R. 2025, *The Astrophysical Journal Letters*, 980, L27

Ji, X., D'Eugenio, F., Juodžbalis, I., et al. 2025a, *MNRAS*, doi: [10.1093/mnras/staf2235](https://doi.org/10.1093/mnras/staf2235)

Ji, X., Maiolino, R., Übler, H., et al. 2025b, *MNRAS*, 544, 3900, doi: [10.1093/mnras/staf1867](https://doi.org/10.1093/mnras/staf1867)

Jones, G. C., Bunker, A. J., Saxena, A., et al. 2024, *Astronomy & Astrophysics*, 683, A238

—. 2025a, *Monthly Notices of the Royal Astronomical Society*, 536, 2355

Jones, G. C., Übler, H., Maiolino, R., et al. 2025b, arXiv preprint arXiv:2509.20455

Juodžbalis, I., Ji, X., Maiolino, R., et al. 2024a, *Monthly Notices of the Royal Astronomical Society*, 535, 853

Juodžbalis, I., Maiolino, R., Baker, W. M., et al. 2024b, *Nature*, 636, 594

Juodžbalis, I., Marconcini, C., D'Eugenio, F., et al. 2025, arXiv preprint arXiv:2508.21748

Kageura, Y., Ouchi, M., Nakane, M., et al. 2025, *ApJS*, 278, 33, doi: [10.3847/1538-4365/adc690](https://doi.org/10.3847/1538-4365/adc690)

Kaspi, S., Maoz, D., Netzer, H., et al. 2005, *The Astrophysical Journal*, 629, 61

Katz, H., Cameron, A. J., Saxena, A., et al. 2025, *The Open Journal of Astrophysics*, 8, 104, doi: [10.33232/001c.142570](https://doi.org/10.33232/001c.142570)

Kauffmann, G., Heckman, T. M., Tremonti, C., et al. 2003, *Monthly Notices of the Royal Astronomical Society*, 346, 1055

Keating, L. C., Bolton, J. S., Cullen, F., et al. 2024, *Monthly Notices of the Royal Astronomical Society*, 532, 1646

Kennicutt Jr, R. C. 1998, *Annual Review of Astronomy and Astrophysics*, 36, 189

Kewley, L. J., Dopita, M. A., Sutherland, R., Heisler, C., & Trevena, J. 2001, *The Astrophysical Journal*, 556, 121

Khanlari, M. M., Gebhardt, K., Wiess, L., Davis, D., & Cooper, E. 2024, *Bulletin of the AAS*, 56

Kim, K., Alavi, A., Snapp-Kolas, C., et al. 2025, arXiv preprint arXiv:2501.07548

Kocevski, D. D., Onoue, M., Inayoshi, K., et al. 2023, *The Astrophysical Journal Letters*, 954, L4

Kocevski, D. D., Finkelstein, S. L., Barro, G., et al. 2025, *ApJ*, 986, 126, doi: [10.3847/1538-4357/adbc7d](https://doi.org/10.3847/1538-4357/adbc7d)

Kokorev, V., Jin, S., Magdis, G. E., et al. 2023a, *The Astrophysical Journal Letters*, 945, L25

Kokorev, V., Fujimoto, S., Labbe, I., et al. 2023b, *The Astrophysical Journal Letters*, 957, L7

Kokorev, V., Chisholm, J., Endsley, R., et al. 2024, *The Astrophysical Journal*, 975, 178

Kokorev, V., Chisholm, J., Naidu, R. P., et al. 2025, arXiv preprint arXiv:2511.07515

Kokubo, M., & Harikane, Y. 2025, *ApJ*, 995, 24, doi: [10.3847/1538-4357/ae119e](https://doi.org/10.3847/1538-4357/ae119e)

Kollatschny, W., Bischoff, K., & Dietrich, M. 2000, *Astronomy and Astrophysics*, v. 361, p. 901-912 (2000), 361, 901

Labbé, I., van Dokkum, P., Nelson, E., et al. 2023, *Nature*, 616, 266

Labbe, I., Greene, J. E., Bezanson, R., et al. 2024, *The Astrophysical Journal*, 978, 92

Lambrides, E., Garofali, K., Larson, R., et al. 2024, arXiv preprint arXiv:2409.13047

Larson, R. L., Finkelstein, S. L., Kocevski, D. D., et al. 2023, *The Astrophysical Journal Letters*, 953, L29

Li, R., Ho, L. C., & Chen, C.-H. 2025, arXiv preprint arXiv:2505.12867

Li, S.-S., Feng, H.-C., Liu, H., et al. 2024a, *The Astrophysical Journal*, 972, 105

Li, Y., Leja, J., Johnson, B. D., Tacchella, S., & Naidu, R. P. 2024b, *The Astrophysical Journal Letters*, 969, L5

Limousin, M., Richard, J., Jullo, E., et al. 2016, *Astronomy & Astrophysics*, 588, A99

Lin, R., Zheng, Z.-Y., Jiang, C., et al. 2025, *The Astrophysical Journal Letters*, 980, L34

Lin, X., Fan, X., Cai, Z., et al. 2025, arXiv e-prints, arXiv:2507.10659. <https://arxiv.org/abs/2507.10659>

Liu, H., Jiang, Y.-F., Quataert, E., Greene, J. E., & Ma, Y. 2025, *The Astrophysical Journal*, 994, 113

Lofthouse, E. K., Fumagalli, M., Fossati, M., et al. 2023, *Monthly Notices of the Royal Astronomical Society*, 518, 305

Lupi, A., Trinca, A., Volonteri, M., Dotti, M., & Mazzucchelli, C. 2024, *Astronomy & Astrophysics*, 689, A128

Ma, Y., Greene, J. E., Setton, D. J., et al. 2025, arXiv preprint arXiv:2504.08032

Mackenzie, R., Fumagalli, M., Theuns, T., et al. 2019, *Monthly Notices of the Royal Astronomical Society*, 487, 5070

Maddox, N., Frank, B. S., Ponomareva, A., et al. 2021, *Astronomy & Astrophysics*, 646, A35

Maiolino, R., Scholtz, J., Curtis-Lake, E., et al. 2024, *Astronomy & Astrophysics*, 691, A145

Maiolino, R., Risaliti, G., Signorini, M., et al. 2025, *Monthly Notices of the Royal Astronomical Society*, 538, 1921

Mason, C. A., Chen, Z., Stark, D. P., et al. 2025, arXiv preprint arXiv:2501.11702

Matthee, J., Naidu, R. P., Brammer, G., et al. 2024, *The Astrophysical Journal*, 963, 129

McClymont, W., Tacchella, S., D'Eugenio, F., et al. 2025, *MNRAS*, 540, 190, doi: [10.1093/mnras/staf745](https://doi.org/10.1093/mnras/staf745)

Miralda-Escudé, J. 1998, *The Astrophysical Journal*, 501, 15

Naidu, R. P., Matthee, J., Katz, H., et al. 2025, arXiv preprint arXiv:2503.16596

Nakajima, K., Ouchi, M., Isobe, Y., et al. 2023, The Astrophysical Journal Supplement Series, 269, 33

Nakane, M., Ouchi, M., Nakajima, K., et al. 2024, The Astrophysical Journal, 967, 28

Newville, M., Otten, R., Nelson, A., et al. 2025, LMFIT: Non-Linear Least-Squares Minimization and Curve-Fitting for Python, 1.3.3, Zenodo, doi: [10.5281/zenodo.15014437](https://doi.org/10.5281/zenodo.15014437)

Pacucci, F., Nguyen, B., Carniani, S., Maiolino, R., & Fan, X. 2023, The Astrophysical Journal Letters, 957, L3

Park, H., Jung, I., Yajima, H., et al. 2025, ApJ, 983, 91, doi: [10.3847/1538-4357/adc001](https://doi.org/10.3847/1538-4357/adc001)

Pérez-Montero, E. 2017, Publications of the Astronomical Society of the Pacific, 129, 043001

Pérez-Montero, E., Amorín, R., Sánchez Almeida, J., et al. 2021, Monthly Notices of the Royal Astronomical Society, 504, 1237

Price, S. H., Bezanson, R., Labbe, I., et al. 2025, ApJ, 982, 51, doi: [10.3847/1538-4357/adaec1](https://doi.org/10.3847/1538-4357/adaec1)

Richardson, C. T., Wels, J., Garofali, K., et al. 2025, ApJ, 993, 154, doi: [10.3847/1538-4357/adf215](https://doi.org/10.3847/1538-4357/adf215)

Rinaldi, P., Bonaventura, N., Rieke, G. H., et al. 2025, ApJ, 992, 71, doi: [10.3847/1538-4357/adfa10](https://doi.org/10.3847/1538-4357/adfa10)

Rusakov, V., Watson, D., Nikopoulos, G., et al. 2025, arXiv preprint arXiv:2503.16595

Scholtz, J., Maiolino, R., D'Eugenio, F., et al. 2025, A&A, 697, A175, doi: [10.1051/0004-6361/202348804](https://doi.org/10.1051/0004-6361/202348804)

Setton, D. J., Greene, J. E., de Graaff, A., et al. 2025, ApJ, 995, 118, doi: [10.3847/1538-4357/ae1500](https://doi.org/10.3847/1538-4357/ae1500)

Silk, J., Begelman, M. C., Norman, C., Nusser, A., & Wyse, R. F. 2024, The Astrophysical Journal Letters, 961, L39

Stalevski, M., Fritz, J., Baes, M., Nakos, T., & Popović, L. Č. 2012, MNRAS, 420, 2756, doi: [10.1111/j.1365-2966.2011.19775.x](https://doi.org/10.1111/j.1365-2966.2011.19775.x)

Stalevski, M., Ricci, C., Ueda, Y., et al. 2016, MNRAS, 458, 2288, doi: [10.1093/mnras/stw444](https://doi.org/10.1093/mnras/stw444)

Tacchella, S., McClymont, W., Scholtz, J., et al. 2025, MNRAS, 540, 851, doi: [10.1093/mnras/staf718](https://doi.org/10.1093/mnras/staf718)

Tanaka, T. S., Akins, H. B., Harikane, Y., et al. 2025, arXiv. org

Tang, M., Stark, D. P., Topping, M. W., Mason, C., & Ellis, R. S. 2024, The Astrophysical Journal, 975, 208

Tasitsiomi, A. 2006, The Astrophysical Journal, 645, 792

Taylor, A. J., Kokorev, V., Kocevski, D. D., et al. 2025, The Astrophysical Journal Letters, 989, L7

Terp, C., Heintz, K. E., Watson, D., et al. 2024, Astronomy & Astrophysics, 690, A70

Treu, T., & Paris, D. 2023, High-level science products produced by the GLASS-JWST team, as described in Paris, et al. 2024 (ADS bibcode: 2023ApJ...952...20P), and in Mascia, et al. 2024 (ADS bibcode: 2024A&A...690A...2M.., STScI/MAST, doi: [10.17909/KW3C-N857](https://doi.org/10.17909/KW3C-N857)

Trussler, J. A., Cameron, A. J., Eisenstein, D. J., et al. 2025, arXiv preprint arXiv:2510.12622

Übler, H., Maiolino, R., Curtis-Lake, E., et al. 2023, Astronomy & Astrophysics, 677, A145

Übler, H., Maiolino, R., Pérez-González, P. G., et al. 2024, Monthly Notices of the Royal Astronomical Society, 531, 355

Vladilo, G. 1999, arXiv preprint astro-ph/9903406

Wang, B., de Graaff, A., Davies, R. L., et al. 2025, ApJ, 984, 121, doi: [10.3847/1538-4357/adc1ca](https://doi.org/10.3847/1538-4357/adc1ca)

Weaver, J. R., Cutler, S. E., Pan, R., et al. 2024, ApJS, 270, 7, doi: [10.3847/1538-4365/ad07e0](https://doi.org/10.3847/1538-4365/ad07e0)

Witstok, J., Jakobsen, P., Maiolino, R., et al. 2025, Nature, 639, 897

Wolfe, A. M., Gawiser, E., & Prochaska, J. X. 2005, Annual Review of Astronomy and Astrophysics, 43, 861–918, doi: [10.1146/annurev.astro.42.053102.133950](https://doi.org/10.1146/annurev.astro.42.053102.133950)

Wright, E. L. 2006, Publications of the Astronomical Society of the Pacific, 118, 1711

Yue, M., Eilers, A.-C., Ananna, T. T., et al. 2024, The Astrophysical Journal Letters, 974, L26

Zhang, Z., Jiang, L., Liu, W., & Ho, L. C. 2025a, The Astrophysical Journal, 985, 119

Zhang, Z., Jiang, L., Liu, W., Ho, L. C., & Inayoshi, K. 2025b, arXiv preprint arXiv:2506.04350

Zhou, S., Sun, M., Zhang, Z., Chen, J., & Ho, L. C. 2025, The Astrophysical Journal, 991, 137

Zhuang, M.-Y., & Ho, L. C. 2023, Nature Astronomy, 7, 1376